Neutron spectroscopic studies of the crystal field in $HoBa_2Cu_3O_x$ $(6 \leq x \leq 7)$

U. Staub, J. Mesot, M. Guillaume, P. Allenspach, and A. Furrer
Eidgenössische Technische Hochschule Zürich, Laboratory for Neutron Scattering, CH-5232 Villigen PSI, Switzerland

H. Mutka
Institut Laue-Langevin, 156 X, F-38042 Grenoble Cedex, France

Z. Bowden and A. Taylor
Rutherford Appleton Laboratory, Didcot, Oxon, United Kingdom
(Received 27 December 1993; revised manuscript received 26 April 1994)

Inelastic neutron scattering has been employed to study in detail the full crystalline-electric-field (CEF) energy-level scheme in the ground-state J multiplet of Ho^{3+} in $HoBa_2Cu_3O_x$ as a function of the oxygen content x. We have been able to resolve ten ground-state transitions for a series of samples covering the superconducting phase as well as the semiconducting one. J mixing and intermediate coupling effects are shown to be necessary to determine unambiguously the nine and five independent CEF parameters of the orthorhombic and tetragonal symmetry, respectively. The large energy shifts and intensity changes of the observed CEF spectra as a function of the oxygen content x are shown to be related predominantly to a charge-transfer process from the chains to the planes, the actual charge transfer being in good agreement with results derived from both bond valence sum considerations for $YBa_2Cu_3O_x$ and similar CEF data for $ErBa_2Cu_3O_x$.

I. INTRODUCTION

In the perovskite-type compounds $YBa_2Cu_3O_x$ (123) $(6<x<7)$ it is well known that the replacement of the Y ions by most of the magnetic rare-earth (R) ions does not have a detrimental effect on superconductivity,[1] in contrast to conventional superconductors. The oxygen stoichiometry has been shown to have a drastic influence on the physical properties. As the oxygen content x decreases from 7 to 6, the 123-type systems show structural transitions, changes in the superconducting transition temperature T_c (two-plateau structure of T_c), as well as a metal-to-semiconductor transition. For most R-substituted compounds, at temperatures below 3 K, transitions to two- and three- dimensional antiferromagnetic order of the R ion sublattice have been reported. Extensive studies performed by means of several techniques such as magnetic[2] and transport[3] measurements, photoemission spectroscopy,[4] neutron diffraction,[5] and particularly neutron crystal-field spectroscopy[6] contributed towards a detailed understanding of the relation between the above-mentioned phase transitions and the superconductivity.

In the 123 compounds the R ions are sandwiched between two superconducting copper-oxide planes. The $(2J+1)$-fold degeneracy of the ground-state J multiplet of the R ion will be partially lifted under the action of the crystalline-electric-field (CEF) potential which in the point-charge approximation is given by

$$V_{\mathrm{CEF}}(\mathbf{r}) = \sum_i \frac{Z_i e |e|}{|\mathbf{r}-\mathbf{R}_i|} , \tag{1}$$

where $Z_i|e|$ denotes the charge at the site $\mathbf{R}_i$ of the ith ligand ion and e is the electronic charge. Equation (1) implies that the CEF energy-level scheme is a direct function of both the structural (denominator) and the charge distribution (numerator) parameters in the vicinity of the R ion. Thus, any modification of the environment of the R ion will significantly affect its energy-level scheme, i.e., the CEF offers a good opportunity and a very clean way to look at the properties of the superconducting planes in the 123 compounds under various conditions (oxygen deficiency, external pressure, Zn or Ni doping of the Cu sites, irradiation, etc.).

Since very detailed information about the CEF interaction can be obtained from inelastic neutron-scattering (INS) experiments, considerable effort has been involved to study the $RBa_2Cu_3O_x$ systems by means of this technique.[6-11] In this paper we present INS experiments on $HoBa_2Cu_3O_x$ $(6<x<7)$. In these compounds the Ho^{3+} ions have a total angular momentum $J=8$. The CEF will completely lift the 17-fold degeneracy of the ground-state multiplet $^5I_8$ in the orthorhombic phase; in the tetragonal phase some singlets will combine to doublet states. We have measured for several oxygen concentrations x ten ground-state CEF transitions and in addition some excited-state CEF transitions. The observed energies are used to determine the CEF potential. This is a complicated task since, firstly, the low symmetry at the rare-earth site (tetragonal for $x \leq 6.4$ and orthorhombic for $x \geq 6.4$) renders difficult a unique determination of the five and nine independent CEF parameters, respectively. More specifically, in the least-squares fitting procedure we need good start values for the CEF parameters which are available from previous studies of the CEF interaction in $HoBa_2Cu_3O_x$.[12,13] Secondly, the large overall CEF splitting of these compounds makes it necessary to

take into account intermediate coupling as well as J-mixing effects in our calculations. It was then possible to determine a unique set of CEF parameters for each oxygen content.

Significant changes have been observed in the CEF parameters as a function of oxygen content x, which cannot be related to structural changes alone. These changes, however, can be explained by introducing the concept of charge transfer from the chains to the planes. Using an effective point-charge model, a quantitatively good agreement is obtained with a similar analysis performed for $ErBa_2Cu_3O_x$ (Ref. 6) as well as bond valence sum arguments,[14] and confirmation is given that the change of T_c is directly connected to the amount of charge being transferred to the planes.

II. EXPERIMENT

The polycrystalline single-phase starting material of $HoBa_2Cu_3O_x$ was prepared by a standard sintering procedure. We treated the powdered material by a temperature-controlled oxygen desorption-absorption procedure to yield final oxygen contents of $x=6.11$, 6.39, 6.49, 6.61, 6.66, 6.89, 7.05. Each sample was characterized by means of both dc magnetic susceptibility and neutron-diffraction techniques. The samples showed the well known two-plateau structure of T_c (Fig. 1),[14] and neutron-diffraction experiments proved the single-phase character of the samples. Only the samples with $x=6.11$ and 6.39 turned out to be nonsuperconducting. The structure investigations were performed at the reactor Sapir at Würenlingen (Switzerland) with use of the double-axis multicounter diffractometer. The structural results are summarized in Ref. 15.

The INS experiments at low-energy transfer ($\Delta E<5$ meV) were performed with use of the triple-axis spectrometer IN2 at the reactor Saphir in Würenlingen. The energy of the outgoing neutrons was kept fixed at 5 meV, giving rise to an energy resolution of 0.15 meV at zero energy transfer. To gain intensity, the measurements were carried out with use of a doubly bent graphite monochromator as well as a horizontally bent graphite analyzer, both with (002) scattering planes. Consequently, no collimations were used from neutron source to detector. A beryllium filter was inserted between sample and analyzer to eliminate higher-order contamination.

For the intermediate energy range (3 meV $<\Delta E<$ 12 meV) we used the time-of-flight (TOF) spectrometer IN4 at the high-flux reactor of the Institute Laue-Langevin (ILL) at Grenoble with incident neutron energy 17.21 meV. We achieved an instrumental resolution full width at half maximum of 0.7 meV at $\Delta E=10$ meV. For the measurements at low- and intermediate-energy transfers the $HoBa_2Cu_3O_x$ powdered samples were enclosed into cylindrical aluminum containers of 10 mm diameter and 50 mm height.

The high-energy transfer ($50<\Delta E<100$ meV) INS experiments were performed with use of the TOF spectrometer MARI at the spallation neutron source ISIS of the Rutherford Appleton Laboratory at Didcot. We used an incident energy of 100 meV in order to achieve an instrumental resolution of less than 2 meV at $\Delta E=70$ meV. In these experiments the samples were filled into a rectangular aluminum container of $65\times65\times5$ mm^3 volume. All the experiments were performed in the temperature range from 1.5 to 10 K with use of a conventional "orange ILL-type" helium cryostat. The raw data have been corrected for absorption, detector efficiency, and background effects using standard procedures.

III. RESULTS

The energy spectra taken at $T=1.5$ K exhibit ten inelastic lines which are considerably separated in energy: we observe three inelastic lines A,B,C in a low-energy window ($\Delta E<5$ meV), three inelastic lines D,E,F in an

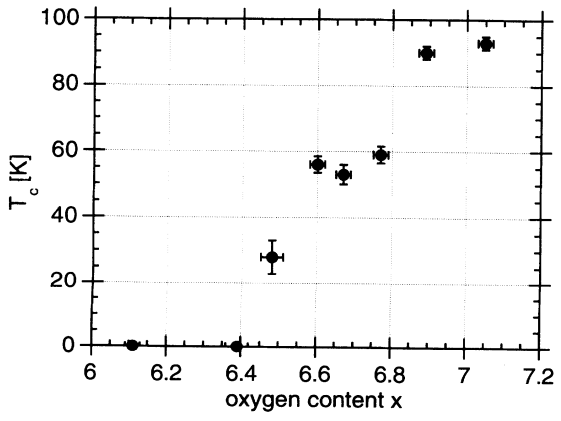

FIG. 1. Superconducting transition temperature T_c vs oxygen content x for $HoBa_2Cu_3O_x$.

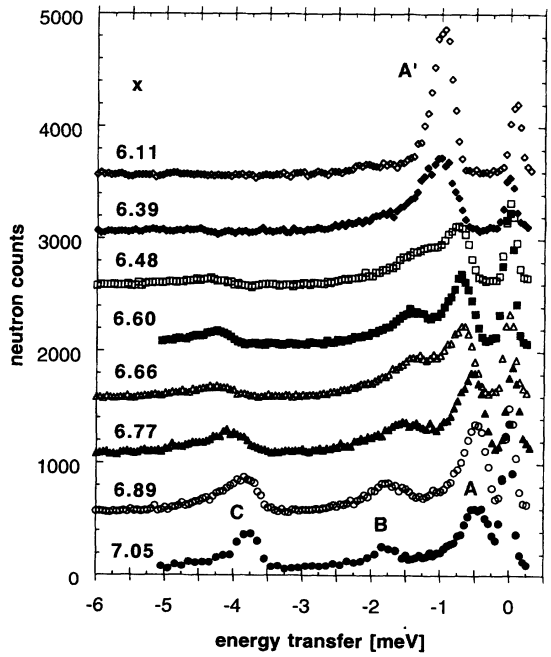

FIG. 2. Energy spectra of neutrons scattered from $HoBa_2Cu_3O_x$ taken on IN2 at $T=1.5$ K, $Q=1.1$ Å^{-1}, and $E_A=5$ meV. To separate the different spectra, the background is consecutively enhanced by 500 neutron counts.

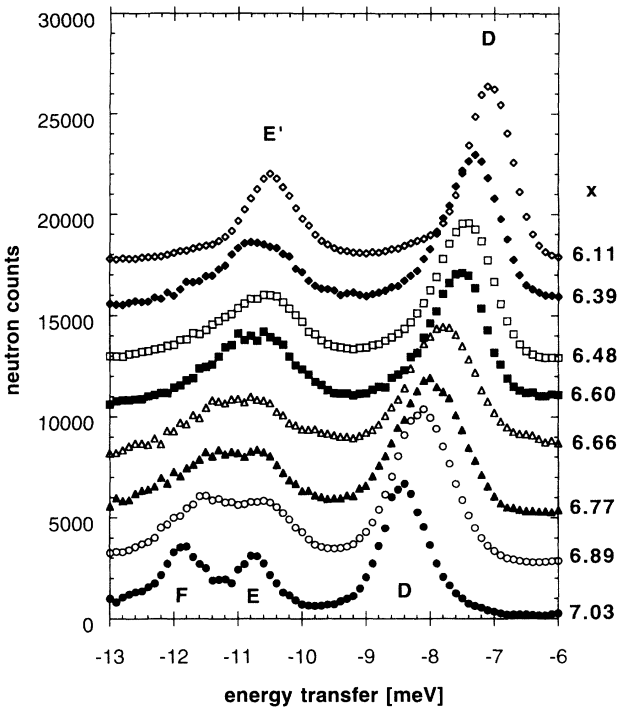

FIG. 3. Energy spectra of neutrons scattered from $HoBa_2Cu_3O_x$ taken on IN4 at $T=2.5$ K, $\langle Q \rangle = 1.3$ Å^{-1} at 8 meV energy transfer and $E_i = 17.21$ meV. To separate the different spectra, the background is consecutively enhanced by 2500 neutron counts.

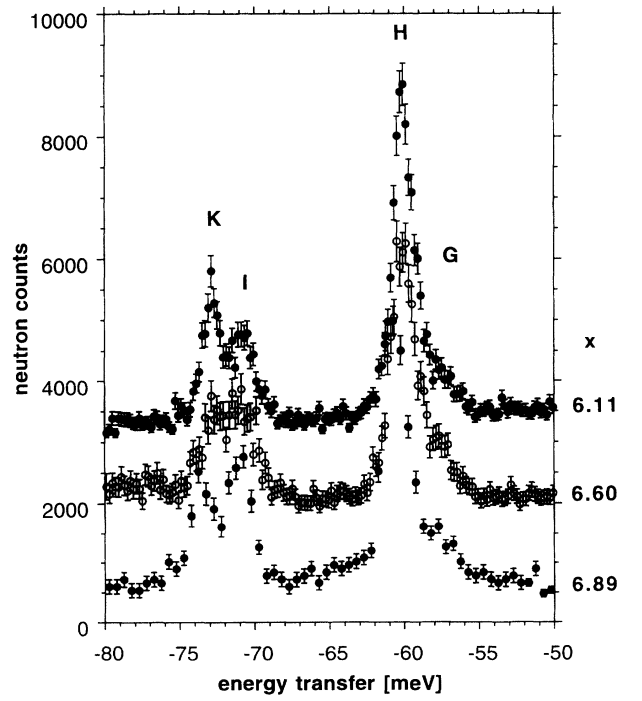

FIG. 4. Energy spectra of neutrons scattered from $HoBa_2Cu_3O_x$ taken on MARI at $T=1.5$ K, $\langle Q \rangle = 2.68$ Å^{-1} at 60 meV energy transfer and $E_i = 100$ meV. To separate the different spectra, the background is consecutively enhanced by 1500 neutron counts.

intermediate-energy window ($5 < \Delta E < 15$ meV), and four lines G,H,I,K in a high-energy window ($55 < \Delta E < 75$ meV) as shown in Figs. 2–4. The gap between the intermediate- and high-energy window is structureless. There is no doubt about the magnetic origin of these inelastic lines, since the intensities observed for the reference sample $YBa_2Cu_3O_7$ turned out to be at least one order of magnitude smaller in these three energy windows. Moreover, the intensities of all the lines followed the magnetic form factor and the Boltzmann statistic, thus we could ensure that they are of magnetic origin. Figure 5 shows the Q dependence of the high-energy transitions of the $x=6.89$ compound, and Fig. 6 shows the temperature dependence of the first-excited transition L in $HoBa_2Cu_3O_{6.11}$. We can thus interpret all ten lines $A-K$ in terms of CEF transitions out of the ground state, since at low temperature ($T=1.5$ K) only the CEF ground state is populated.

Figures 2–4 show the oxygen stoichiometry dependence of the observed energy spectra. When going from $x=7$ to $x=6$, the transitions B,D,F,H,I,K shift slightly to lower energies, the transitions A,C move up to higher energies, whereas the energy of the transitions E,G remains unchanged. At the phase transition from orthorhombic to tetragonal symmetry, some of the CEF transitions merge pairwise into a single line (e.g., $A+B \rightarrow A'$) and some disappear (e.g., C). Note that some transitions (e.g., A,B,C) exhibit an asymmetric line shape. In the data analysis we simply considered the center of gravity and the integrated intensity of each peak. A possible interpretation of the asymmetry of the line shape will be given in Sec. V.

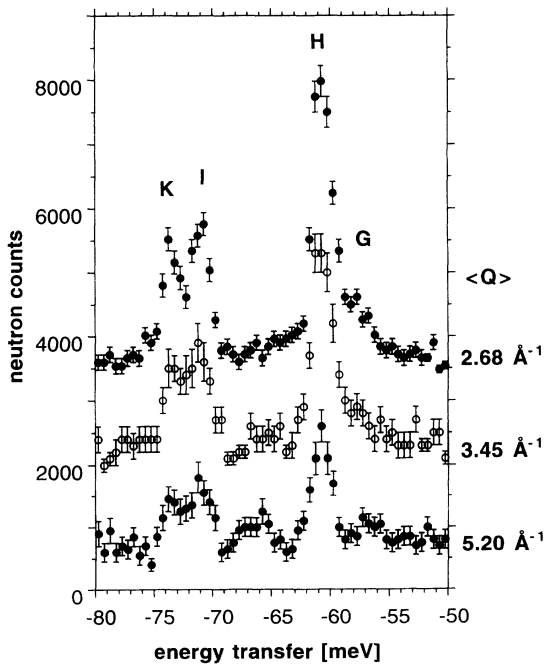

FIG. 5. Q dependence of the MARI data taken for $HoBa_2Cu_3O_{6.89}$ at $T=1.5$ K and $E_i = 100$ meV. To separate the different spectra, the background is consecutively enhanced by 1500 neutron counts.

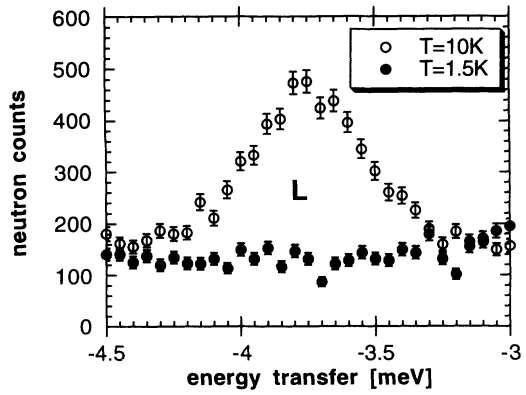

FIG. 6. Temperature dependence of the first excited transition $L\ \Gamma_4^{(1)} \rightarrow \Gamma_3^{(2)}$ taken for $HoBa_2Cu_3O_{6.11}$ on IN2 with $Q=1.1$ Å^{-1} and $E_a=5$ meV.

IV. CRYSTAL-FIELD CALCULATIONS

The degeneracy of the J multiplets of a magnetic ion embedded in a crystal lattice is partly removed by the CEF potential produced by the charge distribution of the surrounding ions. The corresponding CEF potential at the R sites takes the form given by Eq. (1). Using the tensor operator equivalents method we can construct the following Hamiltonian:

$$\mathbf{H}_{\mathrm{CEF}}=\sum_{n=1}^{3}\sum_{m=0}^{n} A_{2n}^{2m}(\mathbf{Y}_{2n}^{2m}+\mathbf{Y}_{2n}^{-2m}) , \tag{2}$$

where the $\mathbf{Y}_{2n}^{2m}$ are spherical tensor operators[16] and the A_{2n}^{2m} denote the CEF parameters.

Usually the CEF potential is treated as a perturbation of the ground-state multiplet $^{2S+1}L_J$ alone, however, Goodman, Loong, and Soderholm[17] have shown that for $HoBa_2Cu_3O_x$ the higher J multiplets have to be taken into account, since the overall CEF splitting is comparable in magnitude to the intermultiplet splittings. Therefore, in the present investigation we have performed a simultaneous diagonalization of the electrostatic, spin-orbit and crystal-field interactions. In the case of $HoBa_2Cu_3O_x$ J mixing enhances the separation between the low-energy ($\Delta E<15$ meV) and high-energy window by typically 5%, and intermediate coupling effects produce changes of the individual CEF energy levels of the order of 1 meV. This is considerably outside our experimental accuracy, thus all the multiplets with $J=8$, 7, 6, and 5 have been included in our calculations.

The energies of both the CEF ground-state transitions $A-K$ and the excited CEF transition L have been considered for the fitting of the CEF parameters, thus the number of observables is sufficient to determine unequivocally all nine CEF parameters in the orthorhombic phase as well as the five parameters in the tetragonal phase. As start values in the least-squares fitting procedure we used the parameters obtained from an earlier study of $HoBa_2Cu_3O_x$.[12,13] We fitted first the two oxygen concentrations $x=6.11$ and $x=7.05$. We obtained a good agreement between the calculation and the experimental data as exemplified for $x=7.05$ in Fig. 7. In particular, the calculated intensities of the CEF transitions approximated by Gaussian lines nicely agree with the observed intensities to within 10%. The resulting CEF energy-level schemes for the two oxygen contents are shown in Fig. 8.

We then used the final parameters of the $x=6.11$ and $x=7.05$ samples as starting values for the other oxygen concentration samples. The final result did not depend on whether we started from the high- or the low-oxygen concentration parameters, showing that we have found the correct set of parameters. The resulting CEF parameters are listed in Table I. The CEF parameters determined for $HoBa_2Cu_3O_x$ are found to vary considerably as a function of oxygen content x, which is quantitatively discussed in Sec. V.

The CEF parameters derived in the present work are clearly more precise then earlier data[12,13] due to the much better energy resolution achieved in the INS experiments as well as the extended Hamiltonian including the electrostatic and spin-orbit interactions. A similar Hamiltonian was used in Ref. 17, however, the proposed set of the CEF parameters considerably differs from that derived in the present work, giving rise to subtle inconsistencies with respect to both the energetic ordering of the CEF levels and the intensities of the CEF transitions.

V. DISCUSSION

In the point-charge approximation, the CEF parameters are explicitly given by

$$A_{2n}^{2m}=e|e|\langle r^{2n}\rangle \sum_i Z_i \gamma_{2n}^{2m}(i) , \tag{3a}$$

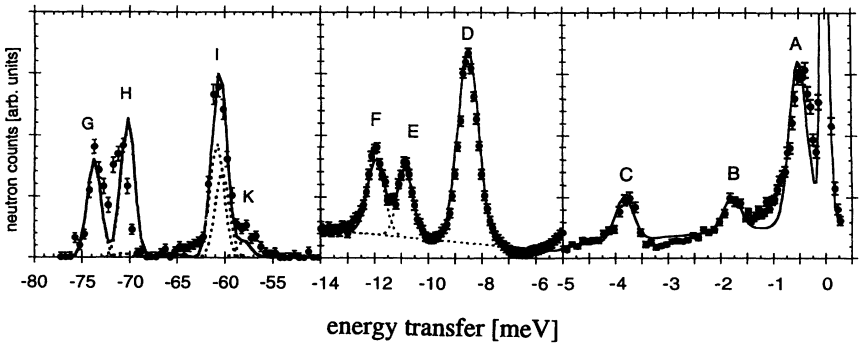

FIG. 7. Energy spectrum of neutrons scattered from $HoBa_2Cu_3O_{7.05}$. Experimental details as in Figs. 2–4. The solid lines correspond to the calculated spectrum. The dashed lines denote the background level and the subdivision onto individual lines.

TABLE I. CEF parameters (in meV) of $HoBa_2Cu_3O_x$ derived in this work.

	A_2^0	A_2^2	A_4^0	A_4^2	A_4^4	A_6^0	A_6^2	A_6^4	A_6^6
7.05	17.6±0.8	12.0±1.0	−34.0±0.2	3.6±0.8	161.3±1.7	3.97±0.05	−2.5±0.8	116.5±0.2	−0.4±0.2
6.89	16.3±0.9	13.7±1.2	−34.1±0.2	0.3±1.1	164.3±1.9	3.95±0.07	−2.4±0.9	117.0±0.2	−0.2±0.2
6.74	14.4±1.0	9.9±1.3	−33.9±0.2	2.8±1.0	165.3±2.1	3.86±0.06	−1.1±0.9	117.1±0.2	0.0±0.3
6.66	14.0±0.9	6.2±1.5	−34.3±0.2	3.1±0.9	164.9±2.1	3.78±0.06	−2.6±0.8	116.8±0.2	0.4±0.3
6.60	13.8±0.8	6.2±1.2	−34.3±0.2	1.7±0.8	165.1±1.9	3.80±0.06	−2.8±1.0	116.7±0.2	0.2±0.3
6.48	10.6±0.9	7.4±1.5	−34.0±0.2	1.3±0.8	169.9±2.1	3.74±0.07	−0.9±0.8	116.7±0.2	0.3±0.4
6.39	8.0±1.1	0	−33.8±0.3	0	169.9±2.7	3.75±0.07	0	116.9±0.3	0
6.11	7.0±0.8	0	−33.8±0.2	0	168.2±2.3	3.68±0.05	0	116.8±0.2	0

with

$$\gamma_{2n}^{2m}(i)=\frac{f_{2n}^{2m}(\theta_i,\phi_i)}{(\mathbf{r}-\mathbf{R}_i)^{2n+1}} \quad . \tag{3b}$$

The sum i runs over all neighboring ions at positions $\mathbf{R}_i=(R_i,\theta_i,\phi_i)$, $\sqrt{4\pi/(4n+1)}f_{2n}^{2m}(\theta_i,\phi_i)$ are tesseral harmonics, $\langle r^{2n}\rangle$ is the 2nth moment of the radial distribution of the $4f$ electrons, Z_i is the charge of the ith ion in units of the electron charge $|e|$, and $\gamma_{2n}^{2m}(i)$ are the geometrical coordination factors as defined, e.g., by Hutchings.[18] Equation (3) shows that the CEF parameters are functions of both the structure and the charge distribution. The point-charge approximation, however, has severe shortcomings and often provides physically unrealistic ligand charges Z_i. This is due to effects such as screening, shielding, antishielding and covalent bonding. To overcome these problems, we proceed in two steps:

(a) As previously[12] shown we can restrict our considerations to the nearest-neighboring oxygen shell, thus Eq. (3) transforms into

$$A_{2n}^{2m}(x)=e|e|\langle r^{2n}\rangle Z(\mathrm{O}(2),\mathrm{O}(3))\gamma_{2n}^{2m}(x) \quad . \tag{4}$$

The geometrical factors $\gamma_{2n}^{2m}(x)$ depend only on the O(2) and O(3) positions.

(2) Considering relative changes of the CEF parameters, we obtain from Eq. (4), assuming only structural modifications:

$$\frac{A_{2n}^{2m}(x)}{A_{2n}^{2m}(7)}=\frac{\gamma_{2n}^{2m}(x)}{\gamma_{2n}^{2m}(7)}\approx\left[\frac{r-R(7)}{r-R(x)}\right]^{2n+1}\leq 1 \quad \text{for } 6\leq x\leq 7 \quad . \tag{5}$$

From the calculation of the geometrical factors we expect a decrease of all the CEF parameters as a function of decreasing oxygen content x.

Figure 9 shows the observed and expected changes of the CEF parameters A_4^0, A_4^4, A_6^0, and A_6^4. Obviously the observed CEF values behave very differently from the values extrapolated according to Eq. (5). The best example is obtained by the behavior of the parameter A_4^4. While the structural parameters are increasing with decreasing oxygen content, the value of the CEF parameter A_4^4 increases, in total contradiction with any structural expectation. This means that structural considerations alone are not sufficient to reproduce these changes. An increase of the charge $Z(\mathrm{O}(2),\mathrm{O}(3))$ upon reduction of the sample could act as a compensation of the structural effects. This is consistent with the idea of charge transfer mentioned by Cava *et al.*,[14] since an increase of the electronic charge $Z(\mathrm{O}(2),\mathrm{O}(3))$ may be interpreted as a decrease of the hole concentration in the CuO_2 planes. In order to quantify these results we consider the point-charge relation

$$A_{2n}^{2m}(x)=e|e|\langle r^n\rangle Z(\mathrm{O}(2),\mathrm{O}(3))[1+\delta(x)]\gamma_{2n}^{2m}(x) \quad , \tag{6}$$

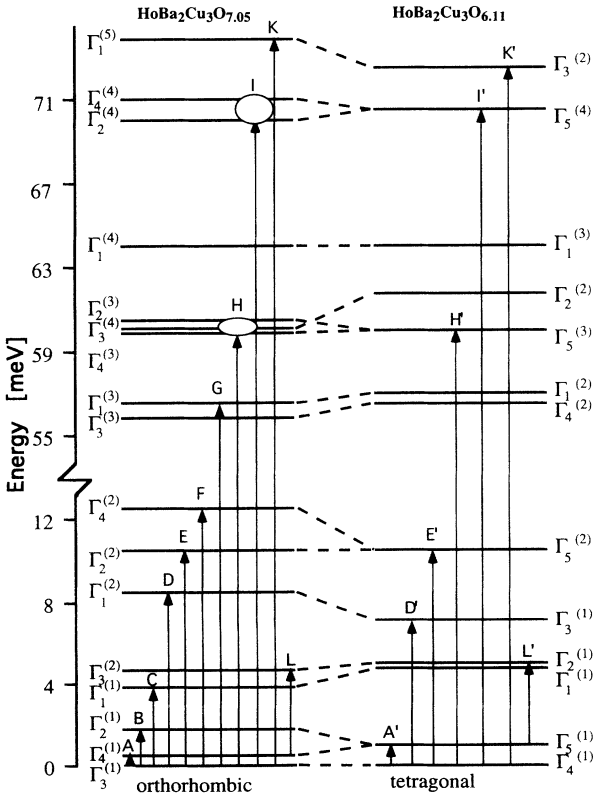

FIG. 8. Energy-level scheme of Ho^{3+} in $HoBa_2Cu_3O_x$ calculated from the CEF parameters for $x=6$ (tetragonal) and $x=7$ (orthorhombic). The arrows denote the observed CEF transitions.

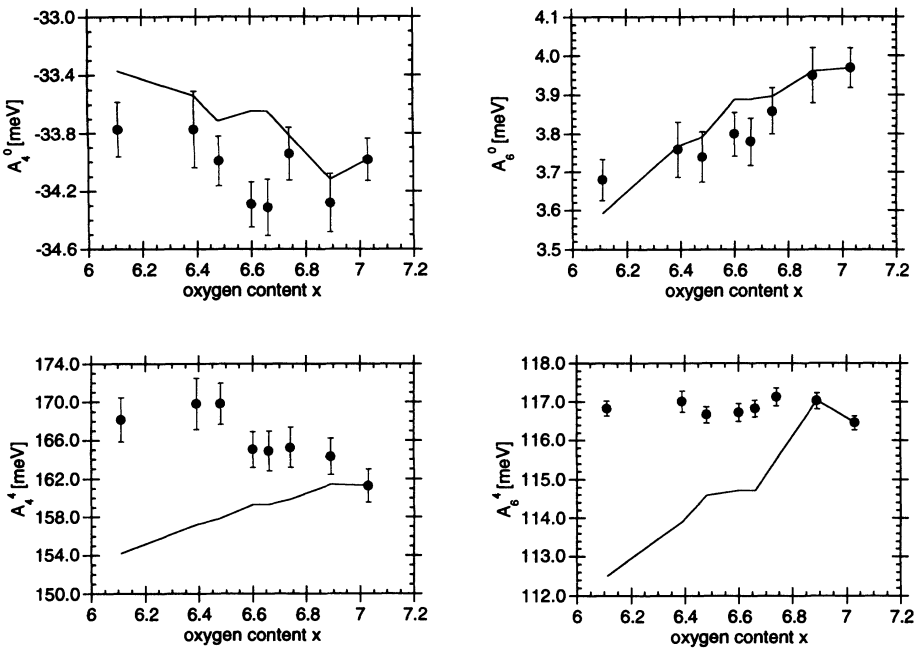

FIG. 9. Leading fourth- and sixth-order CEF parameters determined for $HoBa_2Cu_3O_x$ in this work. The values extrapolated from the structural changes alone are indicated by solid lines.

where $\delta(x)$ describes the relative charge transfer. Taking the compound $HoBa_2Cu_3O_{7.05}$ as a reference [i.e., $\delta(7.05)=0$], a quantitative estimate of the actual charge transfer $Z(\mathrm{O}(2),\mathrm{O}(3))|e|$ can be obtained from Eq. (6):

$$\frac{A_{2n}^{2m}(x)}{A_{2n}^{2m}(7)}=[1+\delta(x)]\frac{\gamma_{2n}^{2m}(x)}{\gamma_{2n}^{2m}(7)} . \tag{7}$$

Since $\gamma_{2n}^{2m}(x)$ is known from crystallographic measurements and $A_{2n}^{2m}(x)$ from CEF spectroscopy, it is very easy to determine $\delta(x)$. We treated in this way only the leading fourth- and sixth-order parameters, since the second-order parameters are long-range parameters and the statistical uncertainty of the remaining "orthorhombic" parameters is rather large. In Fig. 10 we plot the resulting charge transfer $\langle Z|e|\delta(x)\rangle_{mn}$ as a function of the oxygen concentration x [assuming $Z(\mathrm{O}(2),\mathrm{O}(3))=-2$]. We find

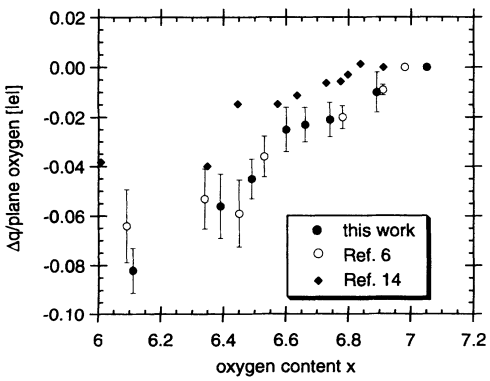

FIG. 10. Charge transfer vs oxygen content x derived for $HoBa_2Cu_3O_x$ in this work, in comparison with similar results obtained for $ErBa_2Cu_3O_x$ (Ref. 6) and for $YBa_2Cu_3O_x$ derived from bond valence sum considerations (Ref. 14).

that a charge of 0.08 $|e|$/O is transferred into the planes when going from $x=6$ to $x=7$, which means that about 32% of the created holes go into the planes, in good agreement with a similar analysis performed for $ErBa_2Cu_3O_x$.[6] This is slightly less than the value of 40% derived from resistivity measurements,[19] and slightly more than the charge transfer 0.04 $|e|$/O (0.08 $|e|$/Cu) derived from diffraction data by means of the bond valence sum formalism[14] for the related Y123 compound.

It is well known that in metallic systems the linewidth of the CEF transitions is connected with the number of carriers.[20] Therefore we expect the linewidths of the CEF transitions to change at $T\approx T_c$ as observed in $TmBa_2Cu_3O_7$.[9] However, upon increasing the temperature the energy spectra of $HoBa_2Cu_3O_x$ become considerably contaminated by excited-state CEF transitions, so that a straightforward interpretation in terms of single Gaussians is no longer feasible.

In the present work we have analyzed the observed energy spectra in an integral manner, i.e., we have not considered deviations from an ideal crystal structure. In fact, the CEF linewidths of the $HoBa_2Cu_3O_x$ compounds with $x=6.11$ and $x=7.05$ (corresponding very closely to the ideal tetragonal and orthorhombic symmetry, respectively) are distinctly smaller than for the intermediate oxygen contents, see Figs. 2–4, which clearly reflects distortions of the local structure. More specifically, a detailed analysis performed for $ErBa_2Cu_3O_x$ (Ref. 7) has shown that the CEF transitions in the 123 high-T_c compounds are composed of a superposition of three components whose spectral weights distinctly depend on the oxygen content x. With the CEF interaction being a local probe, there is no doubt that these substructures originate from different local environments of the R^{+3} ions which obviously coexist in the $RBa_2Cu_3O_x$ compounds and for $R=$Er have been interpreted as being evidence for phase

separation.[7] The spectroscopic information obtained for $HoBa_2Cu_3O_x$ in the present work, however, does not allow such an *a priori* data analysis.

Considering the above comments it is therefore surprising that even for the fully oxygenated compound $HoBa_2Cu_3O_{7.05}$ some CEF transitions are found to exhibit pronounced line-shape asymmetries. Here the superposition hypothesis clearly does not hold. Possible modeling mechanisms in terms of fluctuating fields at the Ho^{3+} sites have recently been discussed.[21]

VI. CONCLUSION

We have presented the results of inelastic neutron-scattering measurements of the CEF transitions of Ho^{3+} and $HoBa_2Cu_3O_x$ for eight different oxygen concentrations. We were able to determine all nine independent CEF parameters in the intermediate coupling approximation including J mixing.

The variation of the CEF parameters with oxygen stoichiometry is shown to be the consequence of a charge transfer from the chains to the planes. We find that the decrease of T_c from 90 to 60 K is associated with a charge transfer of the order of 0.04 e/O, while an additional transfer of 0.04 e/O is needed to reach the insulating state. This type of analysis has been applied to other systems such as $RBa_2Cu_3O_x$ (Ref. 6) (R = Er) and $Nd_{2-x}Ce_xCuO_4$,[22] where similar results were found.

ACKNOWLEDGMENT

Financial support by the Swiss National Science Foundation is gratefully acknowledged.

[1]F. Hulliger and H. R. Ott, Phys. Rev. B **68**, 291 (1987).
[2]S. M. Green, C. Jiang, H. J. Luo, Y. Mei, and C. Politis, Physica C **153-155**, 182 (1988).
[3]R. A. M. van Woerden, H. J. Terpstra, C. F. van Bruggen, M. Kroan, and D. M. de Leeuw, Physica C **170**, 112 (1990).
[4]See, for example, *Electronic Properties of High-T_c Superconductors and Related Compounds*, edited by H. Kuzmany, M. Mehring, and J. Fink, Springer Series in Solid-State Sciences, Vol. 99 (Springer, Berlin, 1990).
[5]J. W. Lynn, T. W. Clinton, W.-H. Li, R. W. Erwin, J. Z. Liu, K. Vandervoort, and R. N. Shelton, Phys. Rev. Lett. **50**, 2606 (1989).
[6]J. Mesot, P. Allenspach, U. Staub, A. Furrer, H. Mutka, R. Osborn, and A. Taylor, Phys. Rev. B **47**, 6027 (1993).
[7]J. Mesot, P. Allenspach, U. Staub, A. Furrer, and H. Mutka, Phys. Rev. Lett. **70**, 865 (1993).
[8]P. Allenspach, A. Furrer, and F. Hulliger, Phys. Rev. B **39**, 2226 (1989).
[9]E. A. Goremychkin, R. Osborn, and A. D. Taylor, Pis'ma Zh. Eksp. Teor. Fiz. **50**, 351 (1989) [JETP Lett. **50**, 380 (1989)].
[10]A. Furrer, P. Allenspach, J. Mesot, U. Staub, H. Blank, H. Mutka, C. Vettier, E. Kaldis, J. Karpinski, S. Rusiecki, and A. Mirmelstein, Eur. J. Solid State Inorg. Chem. **28**, 627 (1991).
[11]L. Soderholm, C.-K. Loong, G. L. Goodman, and B. D. Dabrowski, Phys. Rev. B **43**, 7923 (1991).
[12]A. Furrer, P. Brüesch, and P. Unternährer, Phys. Rev. B **38**, 4616 (1988).
[13]U. Staub, P. Allenspach, J. Mesot, A. Furrer, H. Blank, and H. Mutka, Physica B **180-181**, 417 (1992).
[14]R. J. Cava, A. W. Hewat, E. A. Hewat, B. Battlog, M. Marezio, K. M. Rabe, J. J. Krajewski, W. F. Peck, Jr., and L. W. Rupp, Jr., Physica C **165**, 419 (1990).
[15]U. Staub, Ph.D. thesis No. 10 161, ETH, Zürich, 1993.
[16]B. R. Judd, *Operator Techniques in Atomic Spectroscopy* (McGraw-Hill, New York, 1963).
[17]G. L. Goodman, C.-K. Loong, and L. Soderholm, J. Phys. Condens. Matter **3**, 49 (1991).
[18]M. T. Hutchings, in *Solid State Physics: Advances in Research and Applications*, edited by F. Seitz and D. Turnbull (Academic, New York, 1964), Vol. 16, p. 227.
[19]U. Welp, S. Flescher, W. K. Kwok, J. Downey, Y. Fang, G. W. Crabtree, and J. Z. Liu, Phys. Rev. B **42**, 10 189 (1990).
[20]K. W. Becker, P. Fulde, and J. Keller, Z. Phys. B **28**, 9 (1977).
[21]M. Guillaume, U. Staub, F. Fauth, J. Mesot, A. Furrer, and C. J. Carlile, Physica C **223**, 333 (1994).
[22]A. Furrer, P. Allenspach, J. Mesot, and U. Staub, Physica C **168**, 609 (1990).